Respiratory Physiology & Neurobiology 200 (2014) 110–117

Contents lists available at ScienceDirect

Respiratory Physiology & Neurobiology

journal homepage: www.elsevier.com/locate/resphysiol

Ex vivo bubble production from ovine large blood vessels: Size on detachment and evidence of "active spots"

R. Arieli[a,*], A. Marmur[b]

[a] Israel Naval Medical Institute, IDF Medical Corps, Haifa, Israel
[b] Department of Chemical Engineering, Technion – Israel Institute of Technology, Haifa, Israel

ARTICLE INFO

Article history:
Accepted 29 May 2014
Available online 13 June 2014

Keywords:
Decompression bubble size
Hydrophobic surface
Arterial bubbles
Nucleation
Active spot

ABSTRACT

Nanobubbles formed on the hydrophobic silicon wafer were shown to be the source of gas micronuclei from which bubbles evolved during decompression. Bubbles were also formed after decompression on the luminal surface of ovine blood vessels. Four ovine blood vessels: aorta, pulmonary vein, pulmonary artery, and superior vena cava, were compressed to 1013 kPa for 21 h. They were then decompressed, photographed at 1-s intervals, and bubble size was measured on detachment. There were certain spots at which bubbles appeared, either singly or in a cluster. Mean detachment diameter was between 0.7 and 1.0 mm. The finding of active spots at which bubbles nucleate is a new, hitherto unreported observation. It is possible that these are the hydrophobic spots at which bubbles nucleate, stabilise, and later transform into the gas micronuclei that grow into bubbles. The possible neurological effects of these large arterial bubbles should be further explored.

1. Introduction

It has been shown that tiny, flat gas nanobubbles measuring 5–100 nm form spontaneously when a smooth hydrophobic surface is submerged in water containing dissolved gas (Tyrrell and Attard, 2001; Yang et al., 2007). In our previous studies (Arieli and Marmur, 2011, 2013a), these nanobubbles were shown to be the source of gas micronuclei from which bubbles evolved during decompression on smooth hydrophobic, but not hydrophilic, silicon wafers. We further showed (Arieli and Marmur, 2013b) that hydrophobicity on the luminal aspect of ovine large blood vessels was associated with the formation of bubbles after decompression. In our previous investigation, blood vessels were anaerobically separated from the complete heart and lungs, stretched over microscope slides under saline, compressed and decompressed, and then photographed. We surmised that tiny bubbles too small to be detected visually would rise to the saline–air interface. We therefore focused the camera on the saline–air interface to capture bubbles which floated and expanded there. Bubbles were formed in both the venous (right atrium, pulmonary artery, and superior vena cava) and arterial circulation (aorta, pulmonary vein, and left atrium) throughout a period of 80 min following decompression. The formation of bubbles in the arterial circulation after decompression was a new observation. The risk of neurological outcome should be related to the size of the bubble on detachment, especially when this occurs in the arterial circulation. As the bubble becomes larger, its effect on the central nervous system is more severe.

In our previous investigation (Arieli and Marmur, 2013b), we photographed the six vessels in sequence, so that almost 2 min separated sets of photographs from the same vessel. After detachment, bubbles may shift a little sideways from the point of origin, which might introduce a certain measure of confusion. In the present study, therefore, only one blood vessel was compressed and decompressed at a time, and a complete sequence of photographs at 1 s intervals was thus obtained for each blood vessel. Focusing the camera on the tissue–saline interface, as opposed to the saline–air interface, made it possible to determine bubble size on detachment and the exact location of bubble formation.

2. Methods

2.1. Tissue preparation

The complete heart and lungs from seven slaughtered sheep (taken on separate days) were obtained at the abattoir, and on removal intact from the thoracic cavity were immediately immersed in a cooler filled with saline. In the laboratory, under saline and without any exposure to air, samples (area $9.9 \pm 2.4\ cm^2$,

* Corresponding author at: 118 Rakefet, D. N. Misgav, 20175, Israel. Tel.: +972 77 8100825; fax: +972 4 9801210.
E-mail address: rarieli@netvision.net.il (R. Arieli).

http://dx.doi.org/10.1016/j.resp.2014.05.014
1569-9048/

mean ± SD) from the pulmonary artery (PA), pulmonary vein (PV), aorta (AO), and superior vena cava (VC), were gently stretched on microscope slides using metal clips with the luminal aspect exposed. Two slides were placed without exposure to air on the bottom of two Pyrex bowls (diameter 26 cm, height 5 cm) under 2.5 cm saline. The other two slides were kept under saline in the refrigerator for the next day.

2.2. Protocol

The bowls containing the samples were transferred to two different 150-litre hyperbaric chambers (Roberto Galeazzi, La Spezia, Italy). Because the metal clips tended to rust during the exposure, in order to reduce the oxygen pressure the hyperbaric chamber was initially flushed with nitrogen, and the pressure was also elevated using nitrogen. For the maintenance of pressure we used compressed air. Pressure was elevated at a rate of 100 kPa/min to 1013 kPa (90 m sea water, 10 atmospheres absolute), and remained at that pressure overnight (21.1 ± 1.6 h, mean ± SD). Gas saturation close to the blood vessel after 21 h at 1013 kPa was calculated to be 15% of full saturation using equations for transient heat conduction, replacing temperature and heat conductance by concentration and diffusion constants (Eqs. 5.54 and 5.55, Incropera and DeWitt, 1990). The same value was obtained using finite-element computer simulation of gas transfer from a gas phase through the saline. This gas load is similar to the nitrogen load in various diving protocols. In the morning, one of the chambers was decompressed at a rate of 100 kPa/min. The bowl was placed carefully on a nearby table for photography. We immediately started automated photographing (Canon EOS 500d with macro lens 100 mm F/2.8 EF USM), at 1-s intervals for one hour. After the first 30 min of photography, the battery and memory card were replaced and photography resumed for the second 30 min. The 60-min sampling time was chosen because we found previously (Arieli and Marmur, 2013b) that at this point the rate of bubble production began to drop. At the end of the 60 min of photography, the slides with the tissues were removed and photographed against graph paper for later scaling.

The same protocol was followed for the bowl in the second chamber, for the remaining two blood vessel samples from the same animal, and for the samples from each of the other six sheep.

2.3. Analysis

2.3.1. Diameter on detachment

The photographs of each sample were examined in sequence until detachment of a bubble was observed, and the time was noted. The camera was focused on the tissue–saline interface, and when a bubble detached and started floating upwards it went out of focus (Fig. 1). Photographs were also magnified in a search for detachment of bubbles that were too small to be detected when the whole sample was under observation. In most cases the detached bubble was observed before it burst. We therefore reckoned that a 1-s interval between photographs was sufficiently short to capture detachment. Bubble expansion during one second is negligible, so that if one obtains the diameter within 1 s of detachment, this will be a reliable estimate of the diameter on detachment. Bubbles produced near the edges of the tissue were not taken into consideration, and therefore the last 1 mm to the edge of the tissue was not included in the analysis. The area of the blood vessel samples and the diameter of a bubble just before detachment were measured using an image processing programme (Image-Pro-Plus, Media Cybernetics Inc., Bethesda, MD, USA).

2.3.2. Bubble growth rate

When surface tension and other forces related to gas micronuclei stability play a minor role, the diameter of a bubble should be linearly related to time (Appendix 1). Because the gas tension in the saline decreased with time (due to the release of gas to bubbles and the atmosphere), we selected bubbles which detached from the blood vessels between 10 and 20 min after decompression. The diameter was measured backwards in time from detachment in 1-min intervals.

2.3.3. Analysis of active spots

Most of the bubbles were produced at active spots. The diameter of bubbles released from a specific spot and the time sequence of detachment were recorded for further analysis.

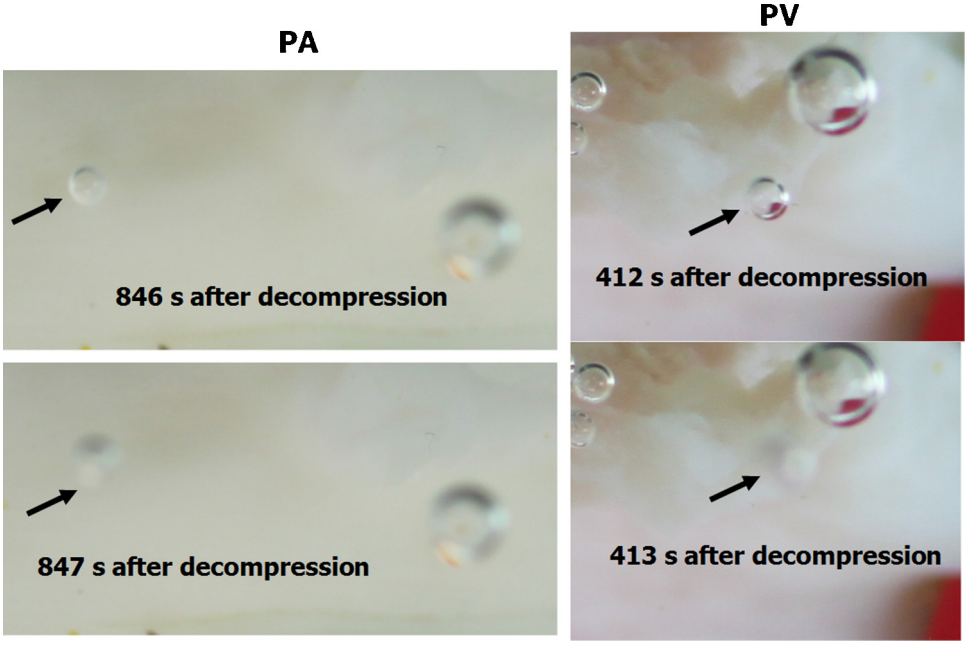

Fig. 1. Detachment of bubbles from the pulmonary artery (PA) and pulmonary vein (PV). After an interval of 1 s, the clearly focused bubble became obscure as it floated upwards.

2.3.4. Calculating the size of the largest bubble as a function of hydrophobicity

Wark (1933) calculated the size of the largest bubble that will adhere at equilibrium to a horizontal, underwater surface having a given hydrophobicity. Hydrophobicity is characterised by the contact angle that a drop of water makes with the surface. A surface is considered hydrophilic if the contact angle is less than 90°, otherwise it is hydrophobic. The calculations were based on the solution of the Young–Laplace differential equation for the shape of an interface under the effect of gravity. It turned out that the size of the largest equilibrium bubble depends only on the surface tension of the liquid and the contact angle with the surface. Thus the size of the largest bubble is a good indication of the hydrophobicity of the surface.

2.4. Statistical analysis

The Kolmogorov–Smirnov test was used for checking normality of the data. One-way ANOVA or the Kruskal–Wallis test were used to examine whether bubble production was the same in the 7 sheep, whether the diameter on detachment differed between blood vessels and between sheep, and whether diameter on detachment differed between spots. When a significant difference was established, a post hoc test was used (Dunnett T4 and Bonferroni), to compare one blood vessel with the others and a single sheep with the others.

3. Results

3.1. Bubble detachment

A bubble could be followed from its first visible appearance until detachment (Fig. 2). Bubble production was highly variable between sheep and blood vessels (Table 1). There seemed to be high bubble production in sheep 3 and 7, and low production in sheep 1, 2, 4 and 5. However, the test for a difference between sheep was not significant ($P = 0.11$). No bubble production was seen in the pulmonary vein of sheep 6 and the pulmonary artery of sheep 5 and 7. Bubble detachment occurred throughout the 1 h of observation, with more during the second half hour – 10 vessels out of 12. There was no statistical difference in the time from decompression until the third bubble detachment: AO – 23.2 min, PA – 16.6 min, PV – 21.8 min, and VC – 20.6 min.

In most cases, there were certain spots at which bubbles appeared either singly or in a cluster. There was clearly no random scattering of bubble production on the luminal surface, rather this was concentrated in spots as exemplified by the three active spots seen in Fig. 3, and an active spot noted at selected times during the photography period shown in Fig. 4. The area of the 15 largest spots is given in Table 2. Large active spots were typical in the aorta and pulmonary artery of those sheep which had high bubble production. Usually, when a bubble which floated to the surface burst, a new bubble could already be seen growing on the tissue.

3.2. Size on detachment

Mean diameter of the bubbles on detachment is shown for the four blood vessels in Fig. 5. Mean detachment diameter was between 0.7 and 1.0 mm. Bubble volume on detachment from the aorta was greater than in the other blood vessels ($P < 0.001$), with no significant difference between the other three vessels. Diameter on detachment differed between sheep ($P < 0.001$), with sheep 7 different from sheep 3, 4, and 5 ($P < 0.001$). Examples of extremely small-sized bubbles on detachment were observed in sheep 6 (PV – 0.17 mm), sheep 7 (VC – 0.2 mm), and another bubble in sheep 7 (VC – 0.2 mm). Extremely large-sized bubbles on detachment were observed in sheep 7 (PA – 4.67 mm), sheep 7 (AO – 1.89 mm), and sheep 3 (PA – 1.68 mm). Because it appeared that bubble nucleation,

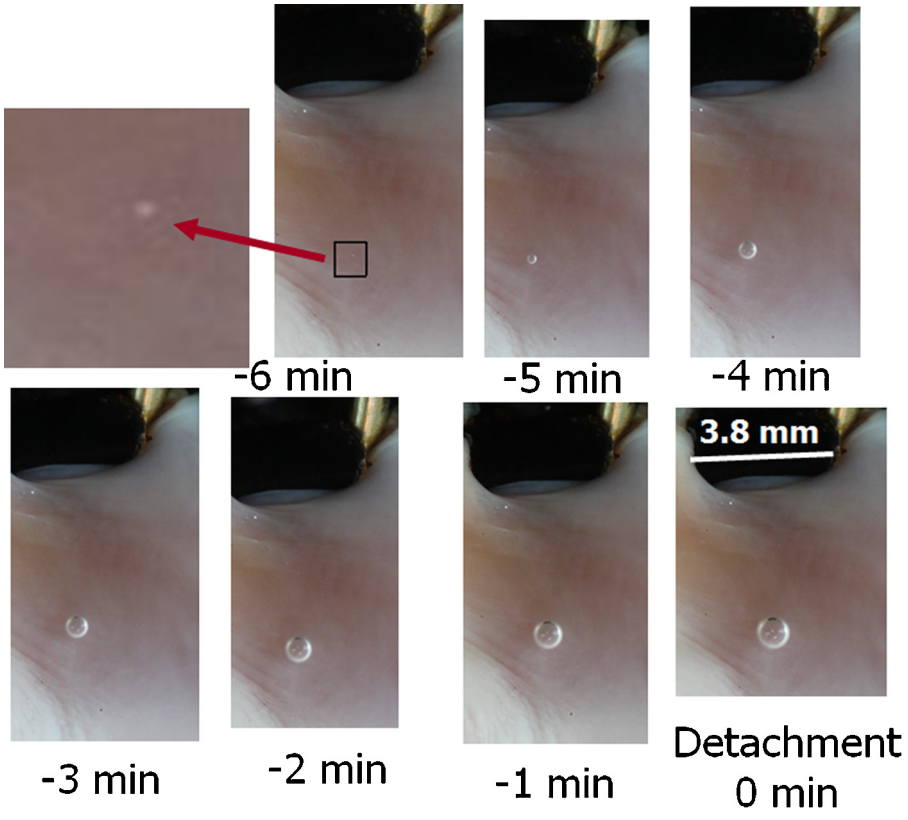

Fig. 2. An example of the first visible bubble on the pulmonary vein, until its detachment.

Table 1
The number of bubbles which detached from the blood vessels of the seven sheep.

Sheep no.	Photography 2 × half hour	AO (bubbles/cm^2)	PV (bubbles/cm^2)	PA (bubbles/cm^2)	VC (bubbles/cm^2)
1	1st	[a]	[a]	0.38	0.08
	2nd	[a]	[a]	0.48	0.38
2	1st	BP	0.64	[a]	[a]
	2nd	BP	[a]	[a]	[a]
3	1st	2.97	2.22	0.41	2.27
	2nd	0.99	4.20	1.91	[a]
4	1st	[a]	0.11	BP	[a]
	2nd	[a]	1.03	BP	0.17
5	1st	0.49	1.05	0.00	[a]
	2nd	1.07	[a]	0.00	[a]
6	1st	[a]	0.00	2.65	0.00
	2nd	[a]	0.00	2.23	0.93
7	1st	0.51	4.62	0.00	0.84
	2nd	2.64	2.83	0.00	2.92

AO, aorta; PV, pulmonary vein; PA, pulmonary artery; VC, superior vena cava; BP, positive bubble production but no counting or measurements.
[a] No data due to technical difficulties.

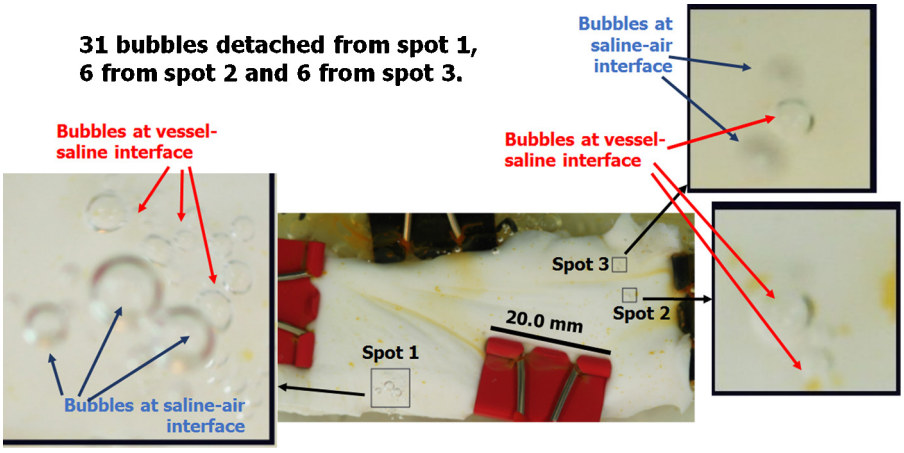

Fig. 3. Bubbles nucleated at three active spots on the aorta of sheep 7. Photo was taken 45 min after decompression.

growth and detachment might be related to physical properties of the active spots, the diameter on detachment is also depicted as a function of the spots (numbered in sequence for each vessel type) in Fig. 6. It can be seen that there were spots from which bubbles detached at smaller diameters than the others ($P < 0.001$).

3.3. Rate of bubble growth

To evaluate whether activation of an active spot influenced its productivity, the time intervals between the detachment of bubbles from the same spot (including time from decompression to the first

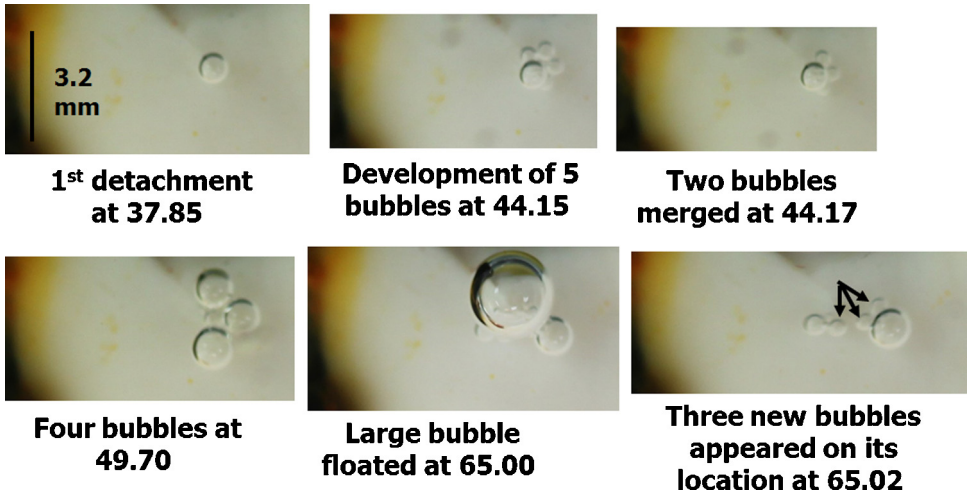

Fig. 4. Snapshots of an active spot on the aorta of sheep 6. Time from decompression in minutes is shown below the pictures.

Table 2
The fifteen largest active spots (in descending order) in the four blood vessels of the seven sheep.

Sheep no.	Blood vessel	Spot area (mm^2)
3	AO	14.8
7	AO	12.3
7	PA	11.7
3	PA	7.5
5	VC	6.7
7	VC	6.2
3	PV	3.6
6	PV	3.5
5	VC	3.0
7	AO	2.9
3	PA	2.8
7	PA	2.7
2	PA	1.6
7	AO	1.2
6	AO	1.1

AO, aorta; PA, pulmonary artery; VC, superior vena cava; PV, pulmonary vein.

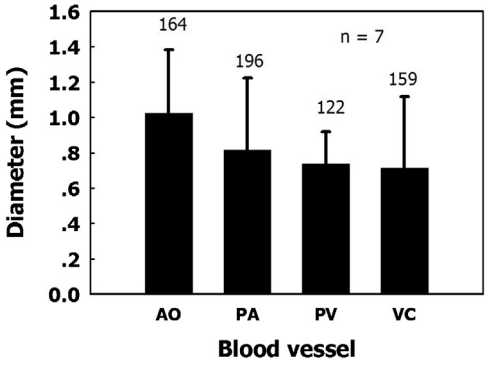

Fig. 5. Diameter of bubbles on detachment (mean ± SD) in the four blood vessels: aorta (AO), pulmonary artery (PA), pulmonary vein (PV), and superior vena cava (VC). Number of bubbles is shown above each column.

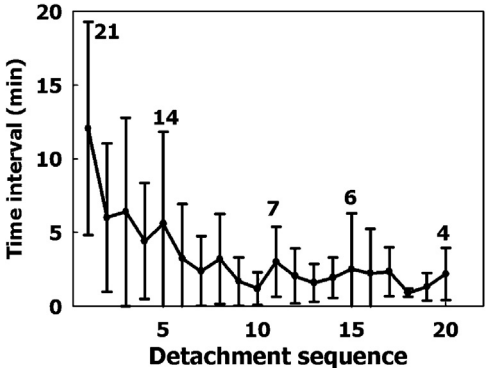

Fig. 7. Time intervals (mean ± SD) between bubble detachments from the active spots. The first value is the time from decompression. Initial number of spots is 21, and the total number decreases with sequence as denoted by the numbers above the symbols.

bubble) were plotted against the sequence of detachments (Fig. 7). Twenty-one spots were selected from the seven sheep and all four types of blood vessel. After decompression, the mean interval to detachment of the first bubble was 12 min, the second detachment took another 6 min, and after the seventh detachment time intervals stabilised at approximately 2 min.

The diameters of 26 bubbles (again selected from all seven sheep and the four types of blood vessel) which detached 10–20 min after decompression were measured at 1-min intervals from detachment back to their first visible appearance (after magnification). The first stages of some bubbles could not be observed, because a previously formed floating bubble from the same site obscured our view. For alignment of the time scale, time 0 was assigned to the point at which the bubble reached a diameter of 0.7 mm. The results are shown in Fig. 8. Bubble diameter increased linearly as a function of time, as expected from the model (Appendix 1). No difference in growth rate was seen between sheep or blood vessels. Extrapolating to the nanobubble scale yielded 8 min to reach a diameter of 0.7 mm from 10^{-6} mm.

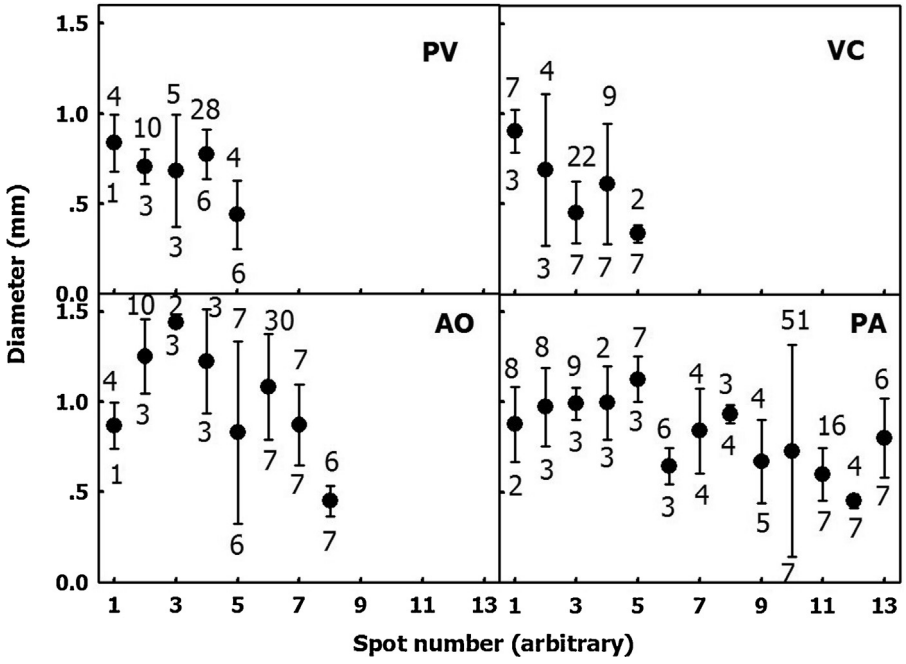

Fig. 6. Diameter of bubbles on detachment (mean ± SD) in the four blood vessels: pulmonary vein (PV), superior vena cava (VC), aorta (AO), and pulmonary artery (PA), for the different active spots numbered in sequence. The number of bubbles is shown above, and the sheep no. below each measurement.

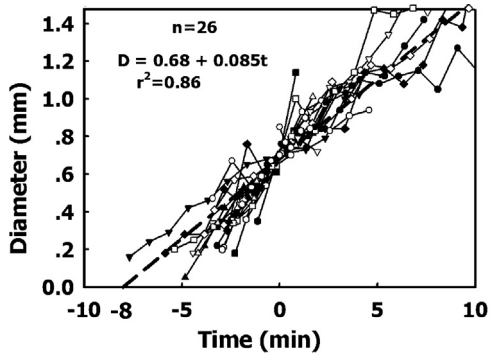

Fig. 8. The growth of bubbles which detached 10–20 min after decompression. The point at which a bubble reached a diameter of 0.7 mm is defined as time 0. Linear regression for all the data is also shown. Each symbol represents a single bubble.

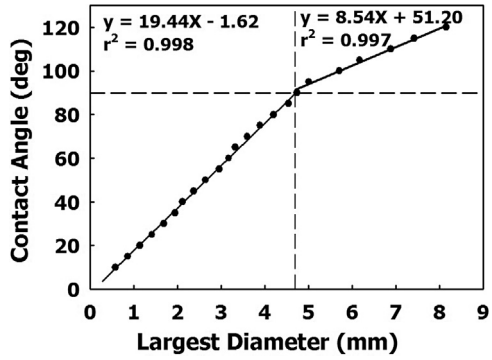

Fig. 9. The size of the largest bubble at equilibrium with water calculated as a function of hydrophobicity (contact angle) of the surface to which the bubble adheres. The dots indicate the calculated theoretical points. The lines are the best straight lines through the theoretical points (separate lines for hydrophilic and hydrophobic surfaces), and are defined by the accompanying equations. The r^2 values show the excellent fit between the lines and the relevant calculated points.

3.4. Size of the largest bubble as a function of surface hydrophobicity

Fig. 9 shows that the angle at the line of contact between the bubble and the solid surface is associated with the largest bubble that will be at equilibrium in water. It can be seen that the curve is very well represented by two straight lines that roughly correspond to hydrophilic and hydrophobic surfaces, where the contact angles are less and greater than 90°, respectively. The largest diameter increases monotonically as the surface becomes more hydrophobic. The largest bubble at the transition from a hydrophilic to a hydrophobic surface (contact angle of 90°) has a diameter of about 4.7 mm.

4. Discussion

In our previous reports (Arieli and Marmur, 2011, 2013a), we showed that nanobubbles which appear on smooth hydrophobic silicon wafers may be the source of gas micronuclei which develop into bubbles on decompression. We further demonstrated that on decompression, bubbles nucleate and expand on the luminal surface of large blood vessels of the sheep (Arieli and Marmur, 2013b). Hydrophobicity was also validated in these vessels. The camera in that study was focused on the saline–air interface, so that it was not possible to determine bubble size on detachment from the surface of the tissue. Focusing on the tissue–saline interface in the present study has enabled us to measure bubble size on detachment.

In the present investigation, blood vessels were studied ex vivo under supersaturated saline. In vivo, with live tissue and blood flow, conditions are liable to be more complex. For example, the possible endothelial production of NO, which was hypothesised to reduce hydrophobicity, would not be present under the experimental conditions of our investigation. It has also been shown that albumin protein sticks to the bubble surface (Miller et al., 1993), which would also not occur in our preparation. It would therefore appear premature at this stage to extrapolate from our results to decompression sickness. However, because blood does not normally contain surfactants, we believe that hydrophobic spots lining the endothelium (Hills, 1992) would be effective in the living organism as well as in the present preparation. The smallest bubble which could be detected on magnification was about 30 μm in diameter, and bubbles could therefore be tracked and followed up above this volume. It was not the purpose of the present study to determine the source of the gas micronuclei.

The development of bubbles in the arterial circulation may have repercussions on certain unresolved questions. Decompression symptoms were unrelated to the bubble score in the venous circulation (Blatteau et al., 2013; Eckenhoff et al., 1986). Whether a smaller number of arterial bubbles can affect decompression symptoms to a greater degree than a higher number of venous bubbles, will depend on their size. Bubbles that detach from the aorta with a diameter of 1 mm may also expand on reaching the nervous system (Imbert et al., 2004). Bubbles carried by the blood into the central nervous system cause the most severe type of neurological decompression illness, as well as serious injury after open heart surgery. Only microbubbles, no greater than 10 μm in diameter, are used in focused ultrasound sonication to open the blood–brain barrier for drug delivery (Choi et al., 2010). A 1 mm bubble is more than 20 times the diameter of a brain arteriole, and can block vital blood supply. Blockage of a single, deep penetrating artery 0.2–0.8 mm in diameter may cause lacunar stroke (Fisher, 1965). The nucleation and detachment of large bubbles in the aorta (and possibly other arteries) may affect the central nervous system, even without arterialisation of venous bubbles which bypass the lung capillaries. Arterialisation was presented by Ljubkovic et al. (2012) and Madden et al. (2013). The possible role of bubbles formed in the arterial circulation would therefore appear to merit further examination.

The normal force of attraction between the surface of the blood vessel and the bubble can be determined from the volume of the bubbles leaving the vessel's surface. Therefore the volume of a bubble (assumed to be spherical) on detachment is calculated as: $(4/3)\pi \times 0.5^3 = 4.6\,mm^3$. The calculated attachment force on detachment is the weight of the displaced water (where a 2.5 cm water column has a negligible effect): $0.46 \times 10^{-5}\,kg = 4.5 \times 10^{-5}\,N$. Bubble diameter was greater on detachment from a hydrophobic silicon wafer (4.2 mm) than on detachment from a blood vessel, and was similar in size to the one and only large bubble (4.67 mm) among all the 641 bubbles observed in the present study. A comparison with the theoretical size on detachment (Fig. 9) shows that the calculated diameter on detachment is close to our previous measurements for silicon wafers (Arieli and Marmur, 2013a). However, bubble diameter was smaller on detachment from the luminal surface of blood vessels. This may be attributed to lower hydrophobicity of the blood vessel or heterogeneity in the hydrophobicity. For example, it may be that the area of the small hydrophobic spot is surrounded by a hydrophilic surface. Once a bubble expands beyond the hydrophobic spot, the force of attraction should be markedly reduced. In our previous study (Arieli and Marmur, 2013a), we showed that the tangential force for detachment from hydrophobic silicon wafers was about half the normal force. If a similar effect operates in real tissue, the tangential force of blood flow would cause detachment of the bubble at a diameter of 0.8 mm compared with 1.0 mm in the presence of a normal force.

The finding of active spots at which bubbles nucleate on the luminal aspect of large blood vessels is a new, hitherto unreported observation. It is possible that these are the hydrophobic spots at which bubbles nucleate, stabilise, and later serve as the gas micronuclei that grow into bubbles. The high variability in hydrophobicity within the same blood vessel reported previously (Arieli and Marmur, 2013b) may be explained by the distribution of the hydrophobic spots.

Further studies are necessary to elucidate the essence of these spots. Because they were identified in the four blood vessels tested, it would seem reasonable that such spots exist at various sites in the vasculature; Hills (1992) demonstrated a phospholipid lining in the brain capillaries of sheep, which may also serve as an active spot. The time intervals between subsequent detachments from an active spot were shorter than the time from decompression to the first detachment (Fig. 7). After the first few detachments, these intervals decreased until they stabilised at a low value. This finding suggests a process of spot activation. Once a spot is fully activated (possible transformation of nanobubbles to gas-micronuclei), bubbles will be produced there at short intervals.

Hills (1992) suggested that the hydrophobicity on the luminal aspect of ovine large blood vessels is due to the deposition of surfactants. Sharma et al. (1996) showed that surfactant adheres to hydrophilic mica in patches. The ionic component attaches to the hydrophilic surface, which leaves the hydrophobic component facing outwards, thus lending hydrophobicity. Lüderitz and von Klitzing (2012) showed that nanobubbles 30–60 nm in diameter are formed on these patches. A similar procedure might have formed the active spots observed in the present study.

Bubble size on detachment in the venous blood vessels was within the high range reported by Hills and Butler (1981), 0.02–0.7 mm. In the present study, we did not observe detachment of bubbles with a diameter less than 0.2 mm in these vessels, while detachment of bubbles with a diameter less than 0.4 mm was a rare occurrence. It is nevertheless a possibility that depending on the tangential force of blood flow and the size and distribution of active spots in small venal vessels, there may be detachment of smaller bubbles.

Once a bubble starts to grow, its radius is linearly related to time (volume is related to time to the power of 3, Appendix 1). The diameter of a bubble increases by 85 μm for each minute. The growth of bubbles from a diameter of 0.1 mm to a diameter of 1.2 mm is calculated to span 13 min. The growth rate within the blood vessels of a living organism may be faster due to the fresh supply of gas-loaded blood, compared with the presumed stratification in our bowl set-up. Nikolaev (2000) calculated that gas micronuclei with a diameter of 1 μm will start to grow on decompression from 100 to 30 kPa. Bubbles appeared, grew and detached throughout the whole hour of our experiment. If it takes 14 min for a bubble to grow from a diameter of 1 μm to 1.2 mm, then the transformation of nanobubbles into gas micronuclei of about 1 μm will be a slower process (Yount, 1989).

5. Conclusion

Bubbles nucleated at specific active spots in all the sheep blood vessels we examined: aorta, pulmonary artery, pulmonary vein, and superior vena cava, and would most probably nucleate in other blood vessels as well. The relevance of these spots to neurological decompression sickness should be further explored.

Acknowledgements

The authors thank Mr. R. Lincoln for skilful editing of the manuscript. This study was supported in part by a grant from the IDF Medical Corps and the Israel MOD (grant no. 1105-2012).

Appendix 1. Rate of bubble growth

V, gas volume; r, radius; t, time; K, permeability coefficient; L, diffusion distance; Pg, gas tension. Bubble is assumed to be spherical.

$$\frac{dV}{dt} = \left(\frac{K}{L}\right)(\Delta \mathrm{Pg}) 4\pi r^2$$

Assuming gas tension difference, permeability coefficient and diffusion distance are constant, then:

$$\frac{dV}{dt} = a 4\pi r^2$$

$$V = \left(\frac{4}{3}\right)\pi r^3$$

$$\frac{dV}{dt} = \frac{d[(4/3)\pi r^3]}{dt} = a 4\pi r^2$$

$$4\pi r^2 \frac{dr}{dt} = a 4\pi r^2$$

$$\int_{r_0}^{R} dr = \int_0^t a\, dt$$

$$R - r_0 = at$$

$$r_0 = 0.000001 \text{ mm} \quad \text{(nanobubble size)}$$

$$R = at + r_0$$

$$V = \left(\frac{4}{3}\right)\pi R^3 = \left(\frac{4}{3}\right)\pi (at + r_0)^3$$

References

Arieli, R., Marmur, A., 2011. Decompression sickness bubbles: are gas micronuclei formed on a flat hydrophobic surface? Respir. Physiol. Neurobiol. 177, 19–23.

Arieli, R., Marmur, A., 2013a. Dynamics of gas micronuclei formed on a flat hydrophobic surface, the predecessors of decompression bubbles. Respir. Physiol. Neurobiol. 185, 647–652.

Arieli, R., Marmur, A., 2013b. Evolution of bubbles from gas micronuclei formed on the luminal aspect of ovine large blood vessels. Respir. Physiol. Neurobiol. 188, 49–55.

Blatteau, J.-E., Brubakk, A.O., Gempp, E., Castagna, O., Risso, J.-J., Vallée, N., 2013. Sidenafil pre-treatment promotes decompression sickness in rats. PLoS One 8 (4), e60639, http://dx.doi.org/10.1371/journal.pone.0060639.

Choi, J.J., Feshitan, J.A., Baseri, B., Wang, S., Tung, Y.-S., Borden, M.A., Konofagou, E.E., 2010. Microbubble-size dependence of focused ultrasound-induced blood–brain barrier opening in mice *in vivo*. IEEE Trans. Biomed. Eng. 57, 145–154.

Eckenhoff, R.G., Osborne, S.F., Parker, J.W., Bondi, K.R., 1986. Direct ascent from shallow air saturation exposures. Undersea Biomed. Res. 13, 305–316.

Fisher, C.M., 1965. Lacunes: small, deep cerebral infarcts. Neurology 15, 774–784.
Hills, B.A., 1992. A hydrophobic oligolamellar lining to the vascular lumen in some organs. Undersea Biomed. Res. 19, 107–120.
Hills, B.A., Butler, B.D., 1981. Size distribution of intravascular air emboli produced by decompression. Undersea Biomed. Res. 8, 163–170.
Imbert, J.P., Paris, D., Hugon, J., 2004. The arterial bubble model for decompression tables calculations. In: Grandjean, B., Méliet, J.-L. (Eds.), Proceedings of the 30th Annual Scientific Meeting of the European Underwater Baromedical Society. EUBS, Ajaccio, Corsica, France, pp. 182–198.
Incropera, F.P., DeWitt, D.P., 1990. Fundamentals of Heat and Mass Transfer, third ed. John Wiley & Sons, New York.
Ljubkovic, M., Zanchi, J., Breskovic, T., Marinovic, J., Lojpur, M., Dujic, Z., 2012. Determinants of arterial gas embolism after scuba diving. J. Appl. Physiol. (1985) 112, 91–95.
Lüderitz, L.A.C., von Klitzing, R., 2012. Scanning of silicon wafers in contact with aqueous CTAB solutions below the CMC. Langmuir 28, 3360–3368.
Madden, D., Lozo, M., Dujic, Z., Ljubkovic, M., 2013. Exercise after SCUBA diving increases the incidence of arterial gas embolism. J. Appl. Physiol. (1985) 115, 716–722.
Miller, R., Policova, Z., Sedev, R., Neumann, A.W., 1993. Relaxation behaviour of human albumin adsorbed at the solution/air interface. Colloids Surf. A: Physicochem. Eng. Aspects 76, 179–185.
Nikolaev, V.P., 2000. Effects of heterogeneous structure and diffusion permeability of body tissues on decompression gas bubble dynamics. Aviat. Space Environ. Med. 71, 723–729.
Sharma, B.G., Basu, S., Sharma, M.M., 1996. Characterization of adsorbed ionic surfactants on a mica substrate. Langmuir 12, 6506–6512.
Tyrrell, J.W.G., Attard, P., 2001. Images of nanobubbles on hydrophobic surfaces and their interactions. Phys. Rev. Lett. 87, 176104-1–176104-4.
Wark, I.W., 1933. The physical chemistry of flotation. I. The significance of contact angle in flotation. J. Phys. Chem. 37, 623–644.
Yang, S., Dammer, S.M., Bremond, N., Zandvliet, H.J.W., Kooij, E.S., Lohse, D., 2007. Characterization of nanobubbles on hydrophobic surfaces in water. Langmuir 23, 7072–7077.
Yount, D.E., 1989. Growth of bubbles from nuclei. In: Brubakk, A.O., Hemmingsen, B.B., Sundnes, G. (Eds.), Supersaturation and Bubble Formation in Fluids and Organisms: An International Symposium. 6–10 June 1988, Kongsvoll, Norway. Tapir Publishers, Trondheim, Norway, pp. 131–164.